Iraqi Journal of Physics, 2026
https://doi.org/10.30723/ijp.v24i3.1550

Vol.24, No.3, PP.39-53
P-ISSN: 2070-4003
E-ISSN: 2664-5548

Structural and Optical Properties of In-Situ Synthesis of PVA/CdS Nanocomposites via Chemical Precipitation-Casting Method

Heidar J. Fadhil[1*] and Haneen T. Hussein[1]
[1]*Department of Physics, College of Science, University of Basrah, Basrah, Iraq*
*Corresponding author: heidar.fadhil@uobasrah.edu.iq

Abstract

Polyvinyl alcohol/cadmium sulfide (PVA/CdS) nanocomposite films were prepared through an in-situ ligand-exchange chemical precipitation-casting method to distinguish the effect of Cd^{2+} complexation from that of CdS nanoparticle formation on the structural and optical properties of PVA. Different volumes (0.25, 0.5, 1, and 2 mL) of cadmium tetraammine complex solution were incorporated into PVA, followed by treatment with ammonium sulfide. The films were characterized using X-ray diffraction (XRD), Fourier-transform infrared spectroscopy (FTIR), and Ultraviolet-visible spectroscopy (UV-Vis). XRD patterns confirmed the formation of nanocrystalline CdS with a hexagonal wurtzite structure and an average crystallite size of approximately 53 nm, while Cd^{2+} coordination reduced the semicrystalline order of PVA. FTIR spectra verified interaction between Cd^{2+} and the hydroxyl groups of PVA and revealed characteristic Cd-S vibration bands, confirming in situ CdS formation. Optical measurements showed that Cd^{2+} complexation produced only minor changes, whereas increasing CdS content markedly enhanced UV absorption and reduced transmittance to approximately 0.5% below 300 nm for the 2 mL sample. The absorption edge shifted from 5.1 to 3.8 eV, and the direct optical band gap decreased from 5.45 to 4.60 eV. These findings demonstrate that in situ CdS formation provides tunable optical and dielectric properties suitable for UV-shielding, photonic, and optoelectronic coating applications.

Article Info.

Keywords:
PVA, PVA/CdS Composite, Optical Properties, Refractive Index, Energy Gap.

Article history:
Received: Jan.29, 2026
Revised: Jun. 29, 2026
Accepted: Jul.10, 2026
Published:Sep.01, 2026

1. Introduction

Metal ion-polymer nanocomposites have received extensive attention due to their adapted properties in solar cells, heavy metal ion removal, photocatalysis, biomedical, gas sensing, and optoelectronics [1], owing to the synergistic combination of the functional versatility of polymers and the unique electronic, optical, and catalytic properties of metal ions or nanoparticles [2]. Enhanced mechanical strength, tailored conductivity, and improved thermal stability arise from metal-polymer duality, making them recommended for a vast range of technological and environmental applications [3].

Cadmium sulfide (CdS) thin film is an n-type semiconductor with a refractive index of 2.5 and a tunable direct band gap transition of 2.1- 3.2 eV [4]. These properties, along with other physical characteristics, are determined by the structural and morphological forms, which result from different preparation methods. The crystalline structure of a semiconductor can be either the wurtzite hexagonal structure or the zinc-blende cubic structure. Chemical co-precipitation has been successfully employed to synthesize single-phase hexagonal CdS nanoparticles with crystallite size of approximately 13 nm [5]. Chemical Bath Deposition (CBD) yields hexagonal and cubic structures when using ammonia and EDTA complexing agents; electrodeposition, hydrothermal, solution growth, solvothermal, chemical spray pyrolysis, and thermally evaporated methods yield hexagonal structures, while biosynthesis yields cubic structures [6, 7]. There are several precursors for cadmium, like cadmium acetate, cadmium sulfate, cadmium chloride, and cadmium nitrate, with average energy band gaps of 2.32, 2.39, 2.47, and 2.55 eV, respectively, while the sulfur precursors are mainly thiourea and ammonium sulfide. The synthesis method and conditions, including complexing

agents, temperature, pH, time, annealing, precursor types, and concentration, play a vital role in the final nanoparticles' structural, morphological, and optical properties [8].

Among various polymers, polyvinyl alcohol (PVA) is widely used as a host matrix because of its optical transparency, water solubility, good film-forming ability, and abundant hydroxyl groups capable of coordinating with Cd^{2+} ions [9]. The -OH functional groups in PVA play a crucial role in chelating metal ions, such as Cd^{2+}. A stable Cd-PVA complex can be produced by coordinating the vacant orbitals of the cadmium ions with the lone-pair electrons of hydroxyl oxygen atoms. This interaction can result in partial or complete ligand exchange, with the original ligands in the Cd complex being replaced or displaced by the hydroxyl functionalities of the polymer. These interactions influence the distribution and binding strength of Cd within the polymer network, resulting in increased structural stability, modified dielectric properties, and improved dispersion of the metal complex throughout the matrix [10]. The PVA/CdS composites alter the absorption and emission characteristics in desirable spectral regions and are appropriate for photonic and photovoltaic applications. The use of CdS nanoparticles as fillers leads to a decrease in the composite band gap, an increase in absorption and refractive index, and the occurrence of photoluminescence representative of quantum confinement and defect states [11–14]. Prior work on CdS/PVA nanocomposites has largely been restricted to standard characterization of fundamental structural and optical properties via XRD, FTIR, and UV-Vis, which only report changes in properties and do not establish mechanistic connections among nanoparticle formation, polymer-nanocrystal interactions, and the resulting optical or dielectric behavior. Alternative synthesis methods, such as gamma irradiation and laser irradiation, have also been investigated, but these are largely empirical trends and do not consider the effects of controlled chemical routes on the nucleation of CdS, its dispersion, and interfacial bonding within the polymer matrix. Few studies to date have distinguished between the effects of CdS incorporation and the formation of CdS nanoparticles within PVA, despite the potential for these two pathways to provide fundamentally different structural environments and electronic responses [10,13,15,16].

In this study, an in-situ ligand-exchange chemical precipitation-casting method is introduced to directly compare PVA-Cd^{2+} complexes and fully developed CdS nanoparticles within the same polymer matrix. This method reveals how Cd^{+2} coordination affects PVA crystallinity, how in situ CdS nucleation alters structural order, and how it causes significant changes in optical absorption, band gap reduction, refractive index augmentation, and dielectric response. Unlike previous reports, this study offers a mechanistic structure-property framework that distinguishes the structural and optical effects of Cd^{2+} complexation from those of CdS nanoparticle formation.

2. Experimental Work

2.1. Materials

PVA powder with a degree of polymerization of 22,500 and a purity of 99% was used in this work. Cadmium acetate, Cd $(C_2H_3O_2)_2.2H_2O$ as Cd^{+2} precursor (from Sigma-Aldrich), and ammonium sulfide $(NH_4)_2S$, as the S2- precursor (BDH Chemicals), at a concentration of 1 g/mL, were used without further treatment or purification.

2.2. Sample Preparation

PVA/Cd^{+2} and PVA/CdS nanocomposites were prepared using the chemical precipitation-casting method. A solution of PVA was prepared by dissolving 2.5 g PVA powder in 200 mL distilled water at 70 °C for 24 hrs with continuous stirring. To prepare a 0.030 M solution of cadmium complex, 0.2 g of cadmium acetate, $Cd(C_2H_3O_2)_2.2H_2O$ (molecular weight 266.53 g/mole), was dissolved in 25 mL of distilled water with continuous stirring for 1 hr, resulting in a clear and transparent solution. Ammonia was then added

dropwise to the solution, where a white, cloudy precipitate formed, which gradually dissolved upon adding excess ammonia, and the solution became clear and transparent once again. PVA/Cd^{+2} samples were synthesized by adding 0.25, 0.5, 1, and 2 mL of cadmium complex solution to 10 mL of dissolved PVA at 25 °C with stirring for 1 hour; the solution was still clear and transparent, and then 0.25 mL of $(NH_4)_2S$ was added to turn the solution into a transparent yellowish color. After that, the solutions were cast in Petri dishes. After 24 hrs, clear and homogeneous films of about 0.5 mm thickness were removed from the Petri dishes.

2.3. XRD Analysis

Bruker D2 Phaser diffractometer equipped with a CuKα radiation source (λ = 1.5406 Å), operated at an accelerating voltage of 30 kV and a current of 10 mA with a 2θ range of 10° to 80°, was used to study the X-ray diffraction (XRD) patterns of the PVA/Cd composite structure. This was done at the University of Basrah, College of Science, Department of Physics.

2.4. FTIR Spectroscopy

ALPHA II Compact Fourier Transform Infrared (FTIR) Spectrometer (Bruker, Germany) was used to investigate the functional groups and chemical interactions within the composite samples. Spectra were recorded in the range of 4000–400 cm^{-1} with a resolution of 4 cm^{-1}. All measurements were carried out at the University of Basrah, College of Science, Department of Chemistry, at room temperature, and the samples were analyzed without any additional preparation to preserve their structural integrity.

2.5. UV–Vis Spectroscopy

The optical properties of the composites were investigated with a UV-Vis spectrophotometer (Shimadzu UV-1800) at the University of Basrah, College of Science, Department of Physics. Measurements were carried out over the wavelength range of 200 - 900 nm at room temperature. The absorption data were used to evaluate the optical refractive index, dielectric constant, and band gap of the CdS nanoparticles using Tauc plots based on the direct-allowed transition model.

3. Results and Discussion

3.1. XRD Characterization

The XRD patterns of the pure PVA, 2 mL Cd complex solution-loaded PVA, and 2 mL Cd complex with ammonium sulfide PVA samples are shown in Fig.1. The figure shows several peak positions that match well with standard data reported in JCPDS No. 80-0006, which corresponds to the hexagonal wurtzite structure of CdS. Specifically, the diffraction peaks observed at 2θ ≈ 24.92°, 26.87°, 28.13°, 36.68, 44.30°, 46.10°, and 49.52° can be indexed to the (100), (002), (101), (102), (110), (103), and (112) planes, respectively. These planes are characteristic of the hexagonal phase and align with previously reported data for wurtzite CdS nanoparticles [15,17].

The presence of the (100), (002), and (101) peaks in the low-angle region is particularly indicative of the wurtzite phase, as these are among the most intense and distinguishable reflections for hexagonal CdS. The peak broadening observed throughout the pattern is consistent with nanocrystalline or size-constrained growth of CdS within the polymer matrix, which inhibits the formation of larger grains. The absence of any additional peaks attributable to the cubic zinc blend phase or secondary phases (e.g., CdO or $Cd(OH)_2$) supports the claim that the synthesized material predominantly exhibits a hexagonal crystalline structure.

Cd Tetraamine complex incorporation into the PVA matrix disturbs the semi-crystalline domain of PVA, leading to coordination with the functional group (–OH),

preventing ordered packing and possibly indicating metal-polymer complexation, as shown in Fig. 1. Despite the low crystallinity, the results indicate a wurtzite hexagonal CdS structure due to light doping and non-annealed samples, which matches the known reference data (JCPDS No. 80-0006).

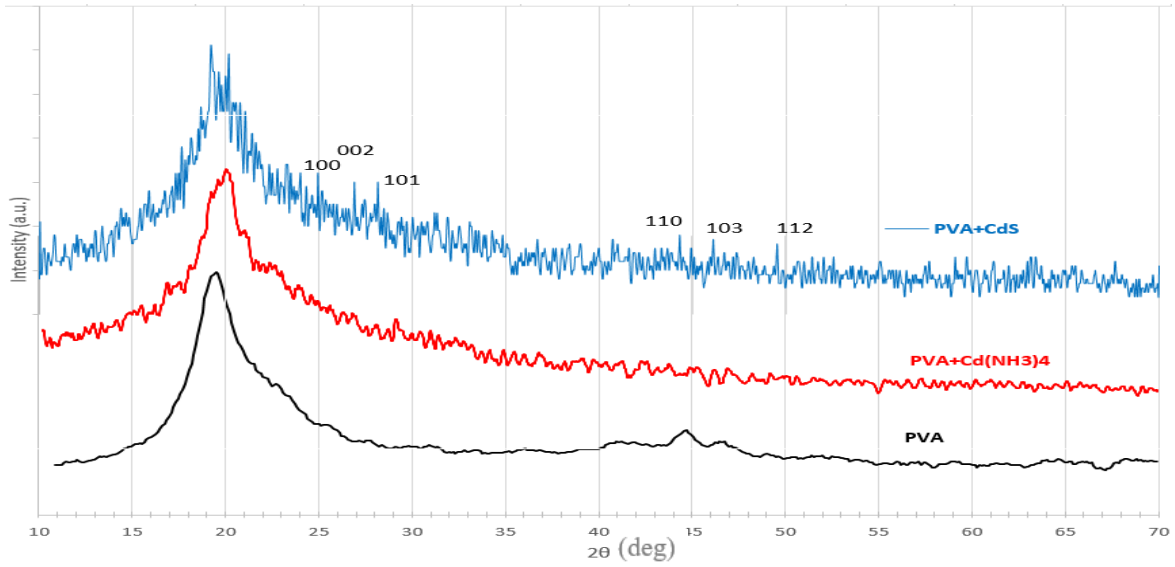

Figure 1: XRD Patterns for PVA, PVA/Cd(NH₃)₄ and PVA/CdS.

To calculate the crystallite size (D) of PVA/CdS, Scherrer's equation was used [18]:

$$D = \frac{K\lambda}{\beta \cos\theta} \qquad (1)$$

where K is 0.94, λ = 1.5045 nm is the X-ray wavelength, and β is the full width at half maximum (FWHM) of the intensity. From the X-ray data, with 2θ = 26.875° and the maximum peak at the 002 plane, the calculated D was equal to 52.98 nm.

3.2. FTIR characterization

Fig. 2 shows the FTIR spectra of the PVA films containing Cd^{+2} ions and CdS nanoparticles. A broad absorption band observed around 3265 cm^{-1} corresponds to O-H stretching vibrations [19] indicating the presence of hydroxyl groups from PVA. The slight shift and broadening of this band suggest hydrogen bonding and potential coordination between Cd^{2+} and –OH groups in the polymer. The bands at 2934 and 1423 cm^{-1} are attributed to C–H stretching and CH_2 bending of the polymer backbone, respectively [19]. A peak near 1518 cm^{-1} may be associated with N–H bending vibrations from coordinated ammonia ligands. The absorption features at 1082 and 1035 cm^{-1} correspond to the C–O stretching mode of PVA. Furthermore, a low-intensity band at 839 cm^{-1} belongs to the skeletal vibration of C-O-C in the acetyl group in the backbone of PVA, while 466 cm^{-1} may be indicative of Cd–O coordination, confirming the successful interaction of the metal complex within the PVA matrix [20].

The FTIR spectrum of the PVA/CdS composite, shown in Figure 2, reveals several characteristic absorption bands that reflect both the polymer matrix and the incorporation of cadmium sulfide nanostructures. A broad band centered at ~3252 cm^{-1} corresponds to the O–H stretching vibrations, indicative of inter- and intramolecular hydrogen bonding within the

PVA backbone[16]. Peaks observed near ~2910–2850 cm^{-1} correspond to C–H stretching of aliphatic –CH_2 groups [16].

The interactions between Cd^{2+} ions and oxygen-containing groups in PVA, such as hydroxyl, are indicated by the sharp bands at ~1701 and ~1651 cm^{-1} [16]. The peaks at ~1421 and ~1243 cm^{-1} can be assigned to CH_2 bending and C–O stretching, respectively [16]. Importantly, the region between ~600–500 cm^{-1} showed weak but distinct absorption bands at 571, 502, and 461 cm^{-1}, which are typically associated with Cd–S stretching vibrations and confirm the formation of CdS nanoparticles within the polymer matrix [16]. The small new peak at 1458 cm^{-1}, shown on the PVA/CdS curve, may be attributed to the interaction of the CdS nanoparticles and the polymer matrix. The observed red shift of the peak at 1559 cm^{-1} in pure PVA to 1518 cm^{-1} upon the addition of Cd^{+2} could be because of the metal coordination to the oxygen of the hydroxyl group [21].

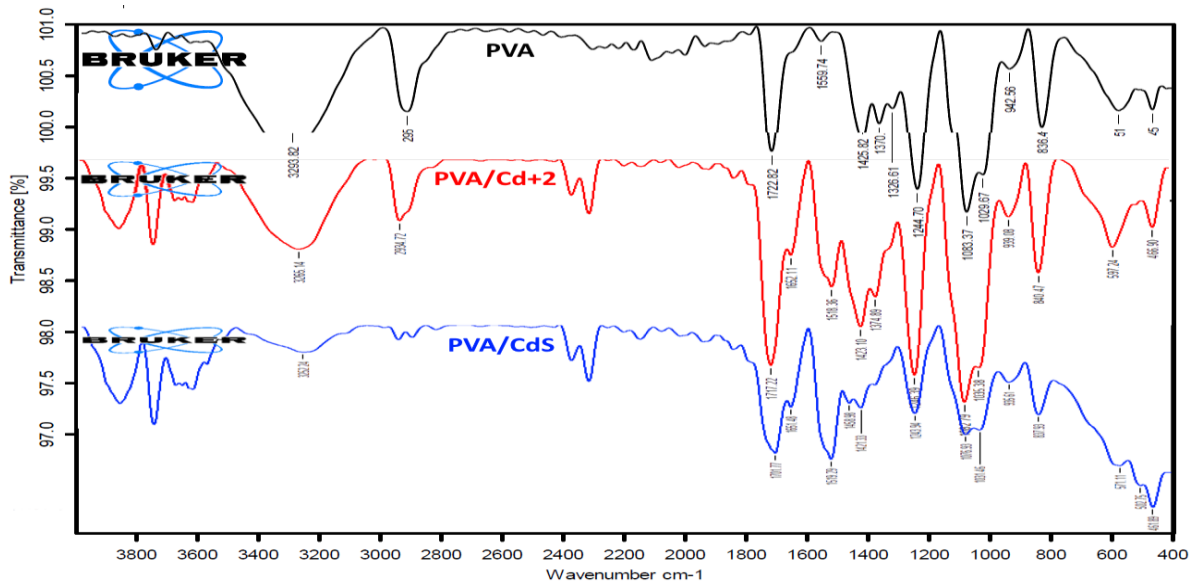

Figure 2: FTIR spectra for pure PVA, PVA/Cd^{+2}, and PVA/CdS.

3.3 Optical Properties

3.3.1 Absorption and Transmission

Fig. 3 shows the optical absorption spectra of pure PVA and Cd^{2+}-doped PVA composites with varying $Cd(NH_3)_4$ concentrations (0.25 to 2 mL). At shorter wavelengths, the absorption intensity increases with Cd^{2+} concentration. This may be attributed to the formation of Cd^{2+}–ligand complexes and their incorporation into the polymer matrix, which introduces localized energy levels and increases UV absorption. At higher doping levels (1–2 mL), a broadening of the absorption edges suggests the onset of charge-transfer transitions between Cd^{2+} and the polymer, contributing to slight redshifts in the band edge [13].

As shown in Fig. 4, the absorption intensity is greatly enhanced compared with that of the Cd^{2+}-PVA samples across the UV region. The absorption peak of the CdS sample 2 mL is more than 4%, nearly twice that of the corresponding Cd^{2+} samples. This remarkable increase can be attributed to the formation of CdS nanoparticles in the PVA polymer, which exhibit strong band-to-band absorption in the UV-Vis region due to quantum confinement effects [22]. The absorption edge shifts slightly to longer wavelengths with increasing CdS concentration, which indicates a narrowing of the optical band gap consistent with the formation of CdS nanocrystals.

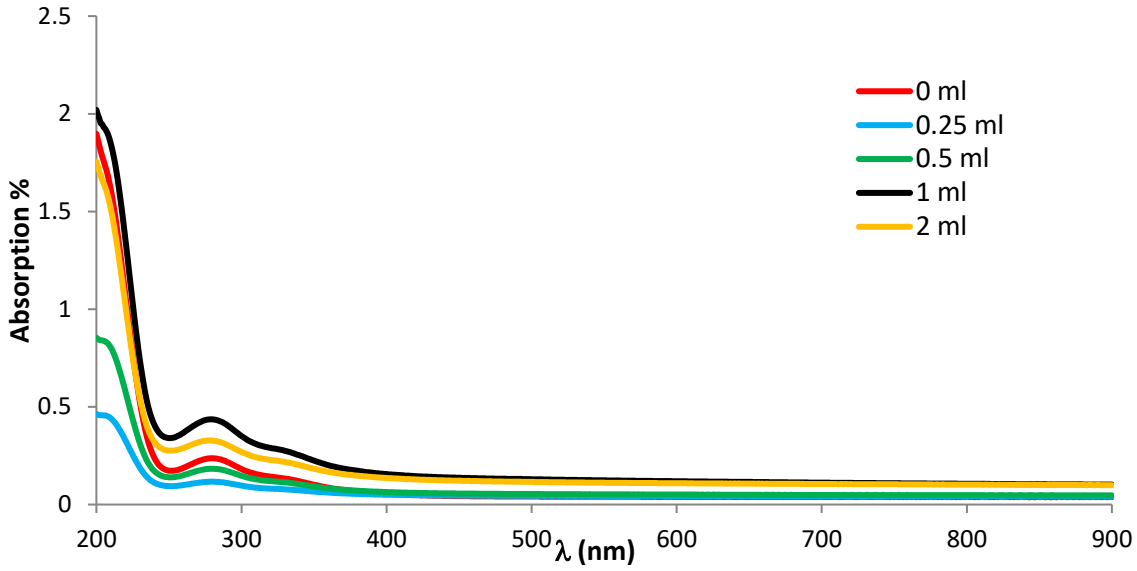

Figure 3: Absorption spectra of pure PVA and PVA/Cd^{+2} doped composites.

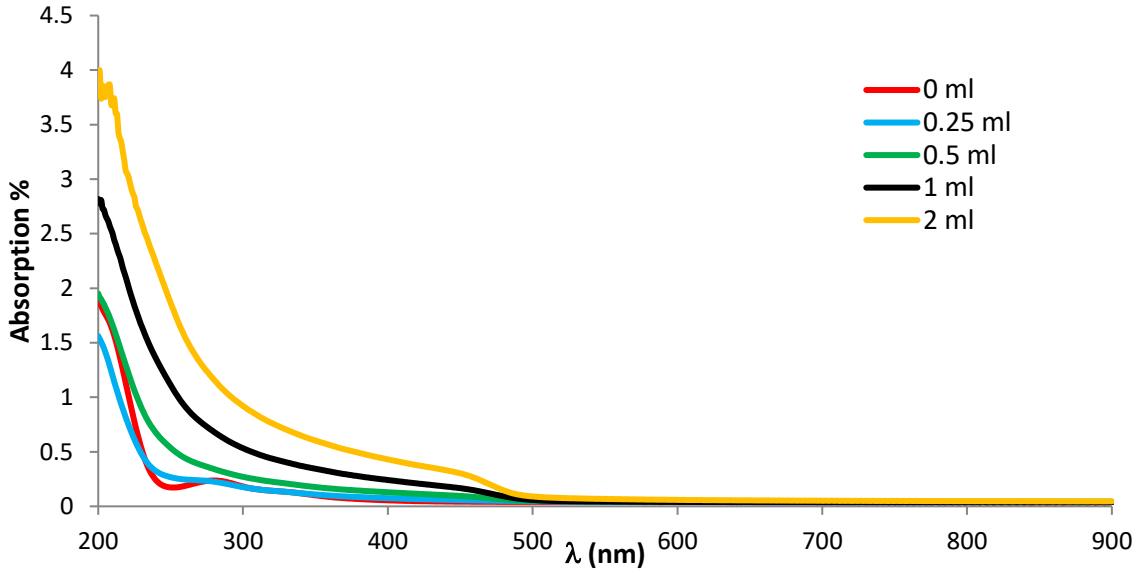

Figure 4: Absorption spectra of pure PVA and PVA/CdS composites.

Fig. 5 displays the transmission spectra of the same PVA/Cd composites, showing a reverse trend. Pure PVA exhibited the highest transmittance (>90%) in the visible region, confirming its optical transparency. But with increasing $Cd(NH_3)_4$ content, the transmittance decreased markedly, especially in the UV region, due to enhanced absorption and possible scattering by cadmium-related species. Transmittance dropped by 60% at 300 nm, which was the most pronounced reduction observed in the 1 and 2 mL samples. Increased electronic absorption from Cd^{2+} complexes and formation of nanostructured domains, which act as scattering centers, can be the reason for this optical attenuation. These changes affirm that Cd^{2+} incorporation modifies the optical density and transparency of the PVA films, making them potential candidates for UV filtering or optoelectronic applications.

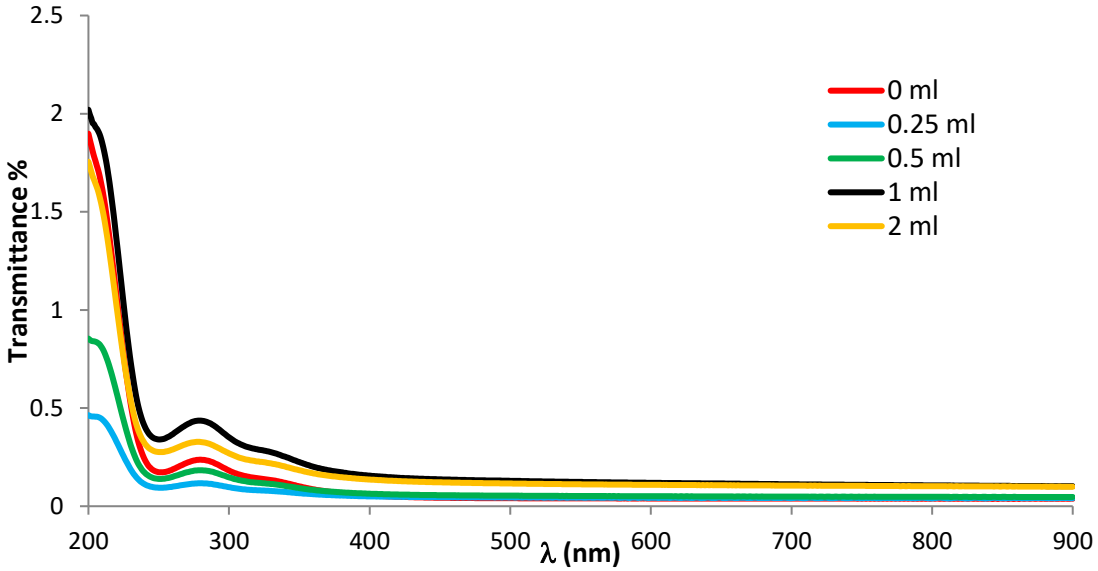

Figure 5: Pure PVA and PVA/Cd^{+2}-doped composites transmission spectra.

The presence of optically active semiconductor phases was confirmed by the transmission behavior of PVA/CdS composites shown in Fig. 6. Pure PVA showed high transmittance throughout the visible spectrum. In contrast, the CdS-doped samples showed suppressed transmittance, especially at lower wavelengths. The lowest transmittance (~0.5% below 300 nm) was observed in the 2 mL CdS sample, indicating a strong UV-blocking potential of the material, far higher than that of the Cd^{2+}-PVA system, where the drop in transmittance was not as severe. The rapid decrease in transmittance with increasing CdS content indicates strong absorption and scattering of photons by CdS nanoparticles; it confirms the incorporation of nanoparticles into the matrix. The results confirmed enhanced optical density in the CdS-PVA films and their potential for UV shielding or optoelectronic coating applications compared with the Cd^{2+}-PVA systems.

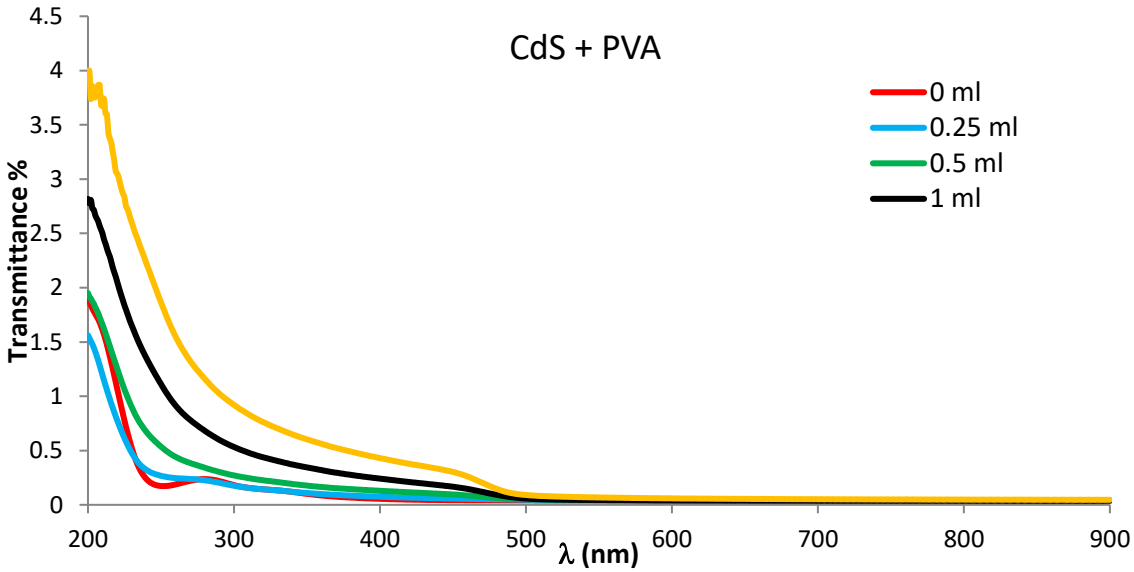

Figure 6: Pure PVA and PVA/CdS composites transmission spectra.

3.3.2 Absorption edge

The absorption coefficient (α) was calculated from the following equation [23]:

$$\alpha = 2.303 \frac{A}{t} \quad (2)$$

where t is the sample thickness, and A is the absorbance. In Eq. 3, transmittance (T) can be calculated from Beer's law:

$$T = 10^{-A} \quad (3)$$

Since all incident light must be either absorbed, reflected, or transmitted, the sum of these components must equal one. Therefore, the reflectance (R), a key parameter for calculating the refractive index, can be readily determined using [24]:

$$R + T + A = 1 \quad (4)$$

The increase of α with increasing dopant concentrations, especially at energies above 6 eV, is shown for the Cd^{2+}-doped PVA composites in Fig. 7. The progressive increase in the absorption edge and the steepening of the curves suggest an increased probability of electronic transitions, which can be attributed to the formation of new localized states or increased interactions between the polymer chains and the Cd^{2+} ions. The PVA/CdS composites, as shown in Fig. 8, exhibited a significant, systematic increase in α across the entire measured spectrum, particularly above 3.8 eV. The significant increase in α with increasing CdS content suggests enhanced light interaction and improved carrier generation, attributable to CdS's semiconductor nature and its ability to absorb in the UV-visible spectrum. Compared to the PVA/Cd^{2+} composites, the PVA/CdS samples exhibited higher absorption coefficients and a significant shift of the absorption edge towards lower photon energies, indicating a reduction in the optical gap and the formation of more efficient optically active centers [25].

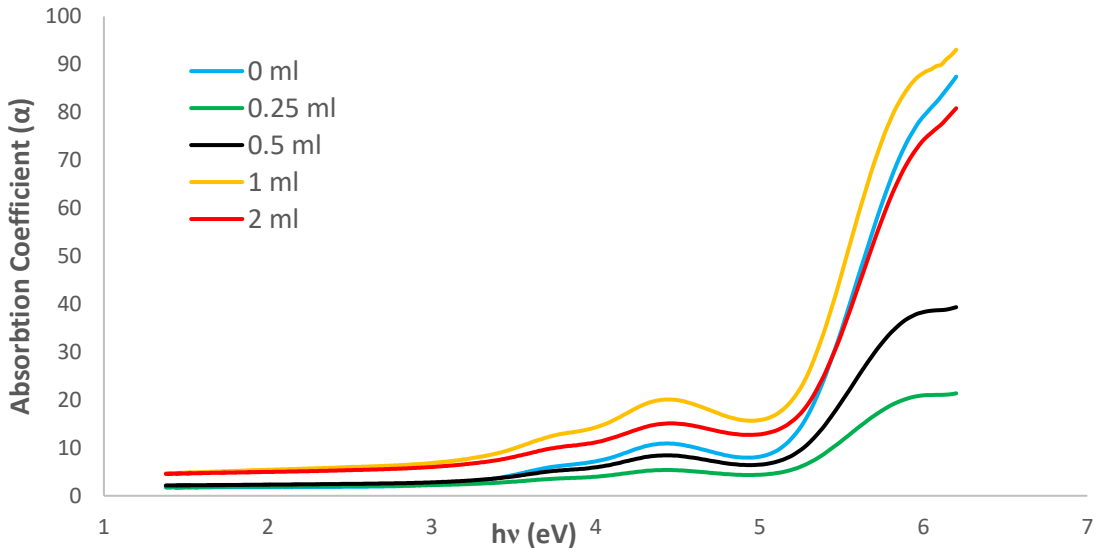

Figure 7: Absorption coefficient vs. photon energy for pure PVA and PVA/Cd^{2+} composites.

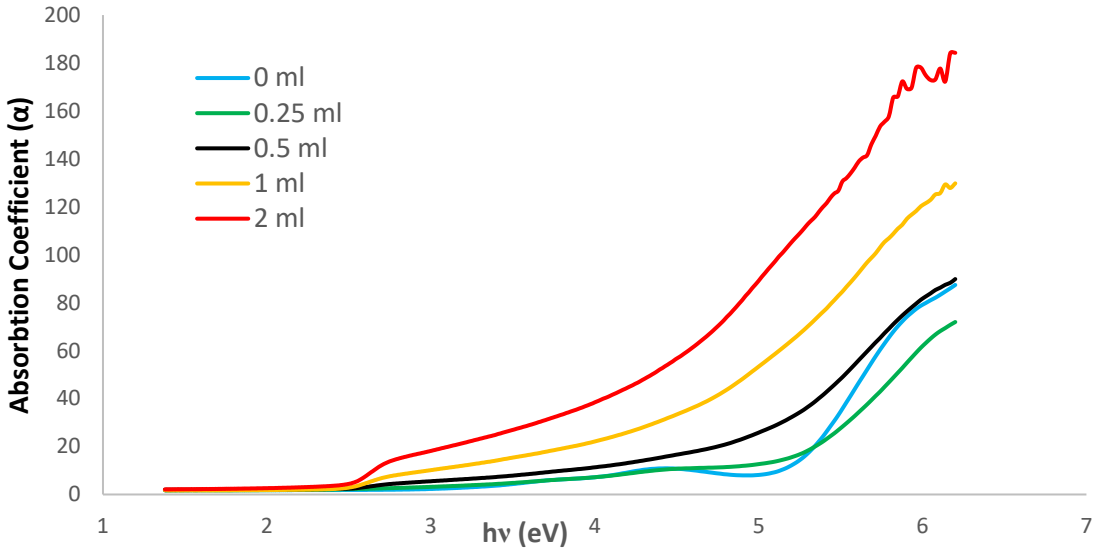

Figure 8: Absorption coefficient vs. photon energy for pure PVA and PVA/CdS composites.

Table 1: Absorption-coefficient energies (eV) for PVA/Cd^{2+} and PVA/CdS composites.

Sample Volume (mL)	PVA/Cd^{2+}	PVA/CdS
0	5.15	5.1
0.25	5.05	5.0
0.5	5.1	4.7
1	5.1	4.3
2	5.15	3.8

The values suggest that incorporating Cd^{2+} ions has minimal impact on the polymer's electronic band structure or on the formation of new energy states within the band gap. The lack of shift indicates weak interaction between Cd^{2+} ions and the PVA matrix in terms of optical transition mechanisms. In contrast, the PVA/CdS composites exhibited a systematic redshift in the absorption edge from 5.1 eV (pure PVA) to 3.8 eV as the CdS concentration increased. This indicates that CdS nanoparticles significantly altered the optical behavior of the host polymer. The reduction in the absorption edge corresponds to a narrowing of the optical band gap, which can be attributed to the formation of new localized states at the polymer–nanoparticle interface, quantum confinement effects, or extended conjugation and charge-transfer interactions. This trend confirms that CdS acts as an active light-absorbing semiconductor, enhancing the polymer's ability to absorb lower-energy photons (visible/near-UV), and making it more suitable for optoelectronic or photonic applications than the inclusion of the relatively inactive Cd^{2+} ion.

3.3.3. Refractive Index

The Refractive index (n) can be calculated from the Fresnel formula [23]:

$$n = \sqrt{\frac{4R}{(1-R)^2} - k^2} + \frac{1+R}{1-R} \qquad (5)$$

where the extinction coefficient (k) can be calculated from [23]:

$$k = \frac{\alpha\lambda}{4\pi t} \quad (6)$$

The refractive index spectra of PVA/Cd^{2+} and PVA/CdS composites are shown in Figs. 9 and ***Figure*** 10, which reveal significant differences in optical behavior. In PVA/Cd^{2+} samples, a moderate increase in refractive index with increasing dopant concentration is observed, showing typical dispersion and saturation near 1.6 at longer wavelengths. The incorporation of CdS into PVA led to more intense peaks and a red shift in the refractive index, demonstrating enhanced light–matter interaction attributed to the semiconductor characteristics of CdS. A maximum refractive index of ~2.7 was exhibited in both systems, but CdS induced more pronounced variations in the UV-visible range. Overall, CdS incorporation led to higher polarizability and tunable optical properties, making it more effective than Cd^{2+} for modifying the refractive behavior of PVA films.

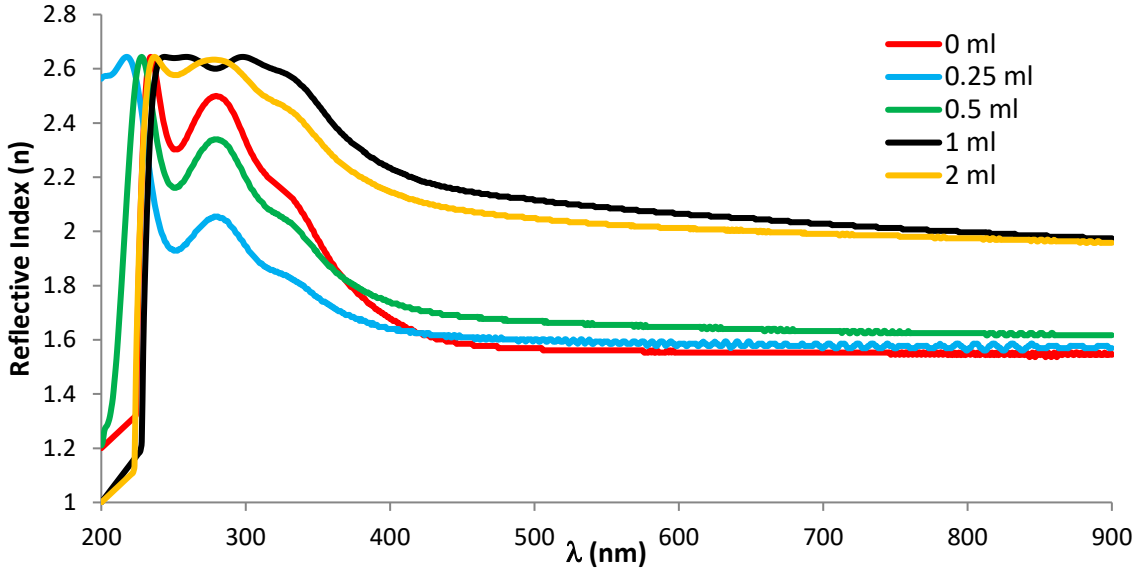

Figure 9: Refractive index for pure PVA and PVA/Cd^{2+} composites.

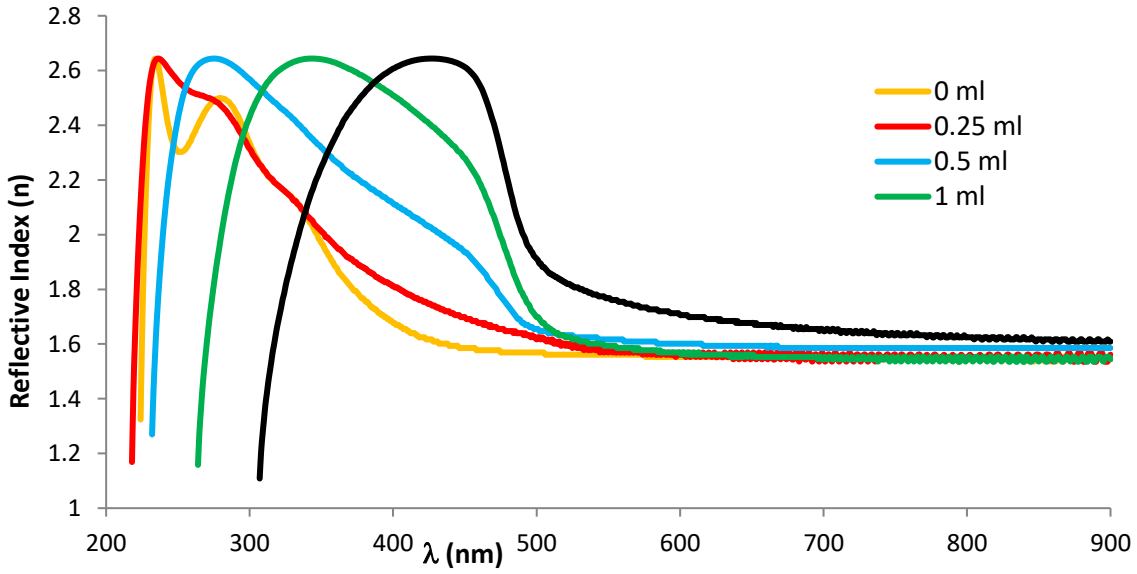

Figure 10: Refractive index for pure PVA and PVA/CdS composites.

3.3.4 Dielectric Constant

The addition of CdS into PVA markedly affected the dielectric constant of the material. Studies indicate that the dielectric properties of polymer composites can be improved through the addition of CdS nanoparticles, leading to notable increases in dielectric constant due to various polarization mechanisms [26]. The dielectric constant (ε_r) can be calculated from the following equation [27]:

$$\varepsilon_r = n^2 - k^2 \quad (7)$$

The dielectric constant of PVA/Cd^{2+} composites showed slight deviation from that of pure PVA, indicating that Cd^{2+} ions did not significantly modify the material's polarizability or electronic structure. This is consistent with the non-semiconducting nature of the Cd^{2+} complex. In contrast, the PVA/CdS composites showed a notable increase and shift of the dielectric peaks with increasing CdS content, especially in the 2-5 eV range. This behavior results from the strong dipole interaction and charge polarization induced by CdS nanoparticles. The enhanced dielectric response confirms the active optical and electronic role of CdS compared to the passive role of Cd^{2+}.

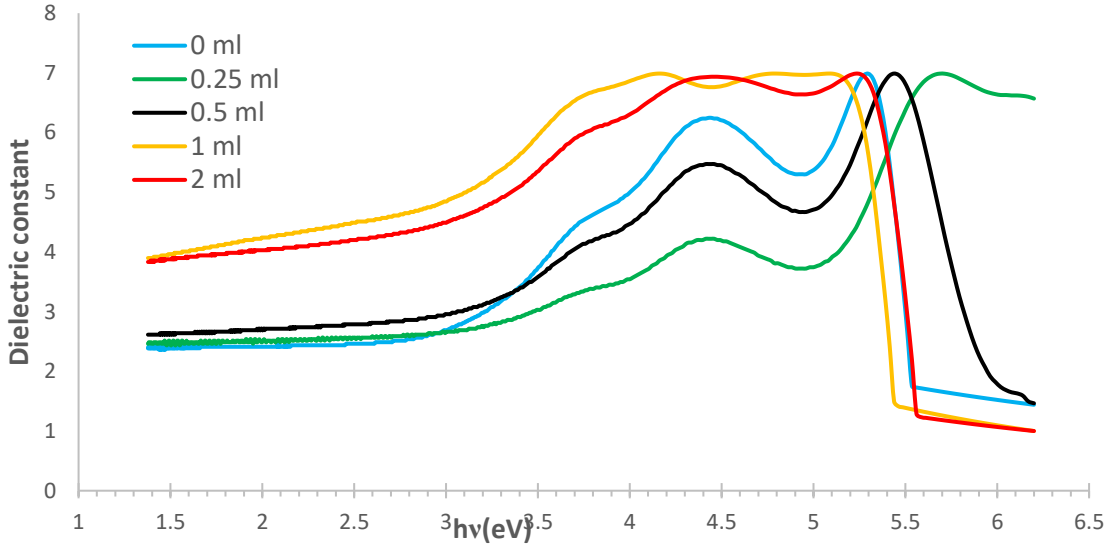

Figure 11: Dielectric constant for pure PVA and PVA/Cd^{2+} composites.

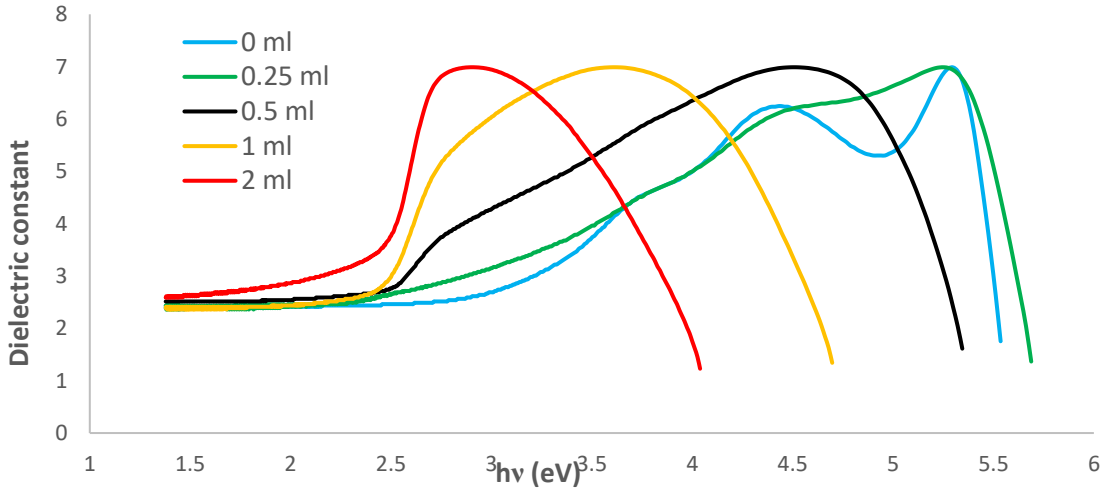

Figure 12: Dielectric constant for pure PVA and PVA/CdS composites.

3.3.5 Band Gap

The energy band gap (E_g) in semiconductors is the energy difference between the top of the valence band and the bottom of the conduction band. It determines the minimum energy needed to excite electrons into a conductive state. This gap governs the material's electrical and optical behavior, influencing charge carrier generation when external energy is applied. Nano-semiconductors with tunable particle sizes and adjustable band gaps can significantly enhance light absorption and exhibit ferromagnetic behavior, making them essential for the development of advanced electronic and photonic devices [28].

Electron transitions in semiconductors occur when photons with energy equal to or greater than the E_g are absorbed, exciting electrons from the valence band to the conduction band. The photon energy $E = h\nu = \frac{hc}{\lambda}$ must match the energy difference between the bands to induce this transition. If the photon energy is lower than the band gap, no electronic excitation occurs. Thus, the onset of optical absorption directly reveals the nature and magnitude of the band gap. The nature of the electronic transition, whether direct or indirect, plays a critical role in determining optical efficiency; in direct transitions, such as those observed in CdS [29], electrons can move between bands without a change in momentum, resulting in stronger optical absorption than in indirect semiconductors. The E_g can be calculated from the following equation, with $\gamma = 1/2$ for direct transitions [30]:

$$E_g = h\nu - \alpha h\nu^{\frac{1}{\gamma}} \quad (8)$$

The Tauc plots of $(\alpha h\nu)^2$ versus $h\nu$, with h as Planck's constant and ν as the photon frequency, for pure and PVA/Cd^{2+} composites in Fig. 13, confirm direct allowed electronic transitions. The estimated optical band gaps for pure PVA and PVA/Cd^{2+} composites are 5.4 eV. This indicates limited electronic interaction between the Cd^{2+} complex and the polymer matrix. Despite the doping, the fundamental nature of the transition remains direct, consistent with the behavior of similar wide-band gap polymeric materials.

The Tauc plots $(\alpha h\nu)^2$ versus photon energy for pure and PVA/CdS composites, as shown in Fig. 14, also confirm the direct allowed electronic transitions characteristic of CdS. A distinct red shift in the optical band gap is observed with increasing CdS concentration, decreasing from ~5.4 eV for pure PVA to ~4.6 eV at a CdS loading of 2 mL, as shown in Table 2. This trend reflects enhanced light absorption and strong interaction between CdS nanocrystals and the PVA matrix. The presence of CdS introduces new energy states that facilitate lower-energy transitions.

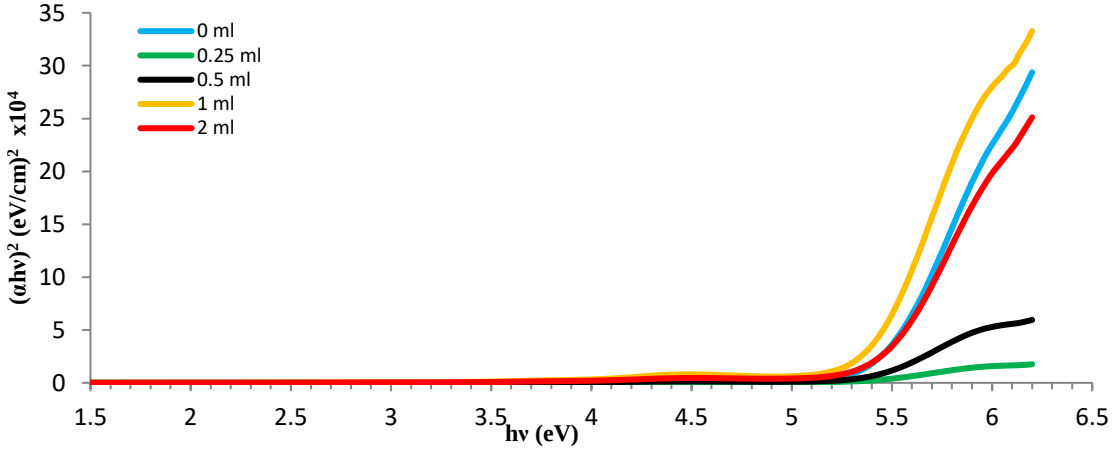

Figure 13: $(\alpha h\nu)^2$ for pure PVA and PVA/Cd^{2+} composites.

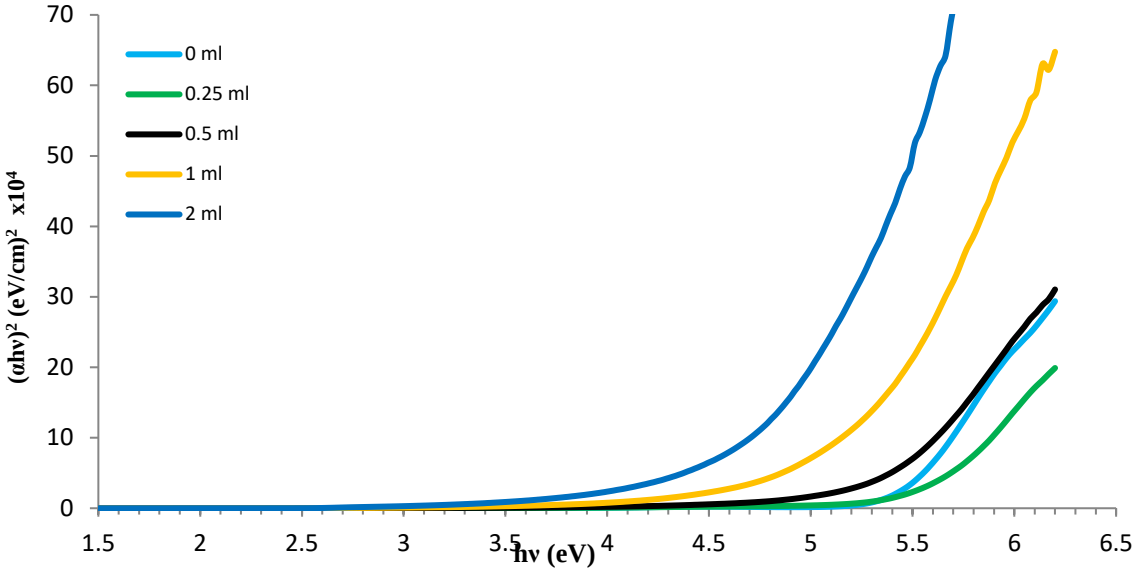

Figure 14: $(\alpha h\nu)^2$ for pure PVA and PVA/CdS composites.

Table 2: Energy gaps (eV) for Cd^{2+} and PVA/CdS composites.

Sample Volume (mL)	PVA/Cd^{2+}	PVA/CdS
0	5.45	5.45
0.25	5.35	5.60
0.5	5.40	5.35
1	5.40	5.20
2	5.40	4.60

4. Conclusions

PVA/Cd^{2+} and PVA/CdS composite films were successfully prepared using an in-situ ligand-exchange chemical precipitation-casting method. Cd^{2+} coordination disrupted the semicrystalline organization of the PVA matrix, while sulfide treatment promoted the formation of CdS nanocrystals. XRD analysis confirmed the formation of nanocrystalline CdS with a hexagonal wurtzite structure. The incorporation of CdS produced greater changes in the optical behaviour than Cd^{2+} complexation, including enhanced absorption, reduced optical transparency, and modified refractive and dielectric responses. Increasing the CdS content further intensified these changes and shifted the optical response toward lower photon energies. Overall, in situ CdS formation was more effective than Cd^{2+} incorporation in modifying the structural and optical behavior of PVA, indicating the potential of these nanocomposite films for UV-shielding and optoelectronic coating applications.

Conflict of Interest

The authors declare no conflicts of interest.

References

1. M. Bulinski, Metal Doped PVA Films for Opto-Electronics-Optical and Electronic Properties, an Overview, *Molecules.* **26**, 2886 (2021). https://doi.org/10.3390/molecules26102886.
2. H. A. Ezzat, M. A. Hegazy, N. A. Nada, O. Osman, and M. A. Ibrahim, Development of natural polymer/metal oxide nanocomposite reinforced with graphene oxide for optoelectronic applications, *NRIAG J. Astron. Geophys.* **10**, 10 (2021). https://doi.org/10.1080/20909977.2020.1846246.
3. E. Salim, A. M. Abdelghany, and A. E. Tarabiah, Ameliorating and tuning the optical, dielectric, and electrical properties of hybrid conducting polymers/metal oxide nanocomposite for optoelectronic applications, *Mater. Chem. Phys.* **313**, 128788 (2024). https://doi.org/10.1016/j.matchemphys.2023.128788.

4. M. Dwivedi, V. Tripathi, D. Kumar, and D. K. Gupta, Structural and morphological characterization of CdS nanoparticles, *Curr. Phys. Chem.* **11**(1), 69 (2021). https://doi.org/10.2174/1877946810999200730222025.
5. B. S. Raq, B. R. Kumar, V. R. Reddy, and T. S. Rao, Preparation and characterization of cds nanoparticles by chemical co-precipitation technique, *Chalcogenide Lett.* **8**(3), 177 (2011).
6. A. Z. Shaikh, S. D. Satpute, J. R. Gadde, R. R. Hawaldar, and K. C. Mohite, Influence of chemical bath deposition temperatures on cadmium sulphide thin film and photosensor application, *ES Materials and Manufacturing*. **20**, 819 (2023). https://doi.org/10.30919/esmm5f819.
7. M. G. Faraj, H. H. Karim, A. F. Qader, I. N. Qader, R. T. Ali. Effect of molarity on the optical and structural properties of CdS thin films deposited by spray pyrolysis on flexible plastic substrates. *J. Mater. Sci: Mater. Electron*. **35**(32), 2069 (2024). https://doi.org/10.1007/s10854-024-13839-z.
8. A. A. I. Lakmal, R. K. K. G. R. G, Kumarasinghe, V. A. Seneviratne, J. Y. Chen, J. M. Song, B. S. Dassanayake. Thermally evaporated CdS thin films for CdS/CdTe solar cells: Effect of substrate temperature on CdS layer. *Mater. Sci. Eng. B.* **273**, 115406 (2021). https://doi.org/10.1016/j.mseb.2021.115406.
9. M.A. Brza, S. B. Aziz, H. Anuar, F. Ali, E. M.A. Dannoun, S. R. Saeed, S. J. Mohammed, R. T. Abdulwahid, Green coordination chemistry as a novel approach to fabricate polymer:Cd(II)-complex composites: Structural and optical properties. *Optic Mater.* **116**, 111062 (2021).https://doi.org/10.1016/j.optmat.2021.111062.
10. H. M. Talib, A. A. Yousif, and A. H. Omran Alkhayatt, Structural, surface morphology and novel gas sensing properties of chemically deposited CdS-PVA nanocomposites; Impact of thiourea content, *Chem. Phys. Impact*. **8**, 100529 (2024). https://doi.org/10.1016/j.chphi.2024.100529.
11. A. Fatemi and M. Rasouli, Engineering Band Gap of Chalcogenide Nanomaterial-Polymer Composites, Meeting Abstracts **MA2022-01**, 2492 (2022). https://doi.org/10.1149/ma2022-01322492mtgabs.
12. N. M. Slaber and J. S. Kith, Optical characterization of PVA/CdS nanostructure. *Exp. Theo. NANOTECHNOLOGY*. **9**(1), 9 (2025). https://doi.org/10.56053/9.1.9.
13. A. Raj, P. K. Singh, S P Pandey, A. Saxena, and B. Bhattacharya, Effect of CdS on the electrical conductivity of polyvinyl alcohol (PVA) and potassium iodide (KI) thin films. *Power System Technology*. **48**(1), 1054 (2024). https://doi.org/10.52783/pst.370.
14. A. Nain, S. Dahiya, R. P. Chahal, and E. Dhanda, Synergic effect of CdS nano additives and UV exposure on properties of PVA/CdS nanocomposite, *ECS Journal of Solid State Science and Technology*. **12**(2), 023008 (2023). https://doi.org/10.1149/2162-8777/acb79d.
15. V. Mohanraj, R. Jayaprakash, P. Sangaiya, S. Gopi, R. Dilip, and R. Suresh, Study of photocatalytic activity and inherent property of surfactant (PVA) on CdS nanoparticles by ultrasonic wave irradiation method, *Int. J. Hydrogen Energy* **42**(47), 28266 (2017). https://doi.org/10.1016/j.ijhydene.2017.09.094.
16. J. Koteswararao, S. V. Satyanarayana, G. M. Madhu, and V. Venkatesham, Estimation of structural and mechanical properties of Cadmium Sulfide/PVA nanocomposite films, *Heliyon.* **5**(6), e01851 (2019). https://doi.org/10.1016/j.heliyon.2019.e01851.
17. M. Milani, M. Mazzanti, G. Magnacca, S. Caramori, and A. Molinari, A Novel hydrothermal CdS with enhanced photocatalytic activity and photostability for visible light hydrogenation of azo bond: synthesis and characterization. *Nanomaterials*. **13**(3), 413 (2023). https://doi.org/10.3390/nano13030413.
18. S. Fatimah, R. Ragadhita, D. F. A. Husaeni, and A. B. D. Nandiyanto, How to Calculate Crystallite Size from X-Ray Diffraction (XRD) using Scherrer Method, *ASEAN J. Sci. Eng.* **2**, 65 (2021). https://doi.org/10.17509/ajse.v2i1.37647.
19. M. A. Brza, S. B. Aziz, H. Anuar, F. Ali, E. M. A. Dannoun, S. J. Mohammed, R. T. Abdulwahid, and S. Al-Zangana, Tea from the drinking to the synthesis of metal complexes and fabrication of PVA based polymer composites with controlled optical band gap. *Sci. Rep.* **10**, 18108 (2020). https://doi.org/10.1038/s41598-020-75138-x.
20. P. L. Reddy, K. Deshmukh, T. Kovářík, N. A. Nambiraj, and K. P. Shaik, Green chemistry mediated synthesis of cadmium sulphide/polyvinyl alcohol nanocomposites: Assessment of microstructural, thermal, and dielectric properties, *Polym. Compos*. **41**(5), 2054 (2020). https://doi.org/10.1002/pc.25520.
21. S. A. Zagorskaya and O. N. Tretinnikov, Infrared spectra and structure of solid polymer electrolytes based on poly(vinyl alcohol) and lithium halides, *Polym. Sci. Ser. A.* **61**, 21 (2019). https://doi.org/10.1134/S0965545X19010115.
22. V. Lahariya, Study of electroluminescence in cadmium sulfide polymer nanocomposite films, *J. Nano Res.* **49**, 181 (2017). https://doi.org/10.4028/www.scientific.net/JNanoR.49.181.
23. S. Mahjabin et al., Investigation of morphological, optical, and dielectric properties of RF sputtered WOx thin films for optoelectronic applications, *Nanomaterials*. **12**(19), 3467 (2022). https://doi.org/10.3390/nano12193467.
24. O. G. Abdullah and D. R. Saber, Optical absorption of polyvinyl alcohol films doped with nickel chloride, *Appli. Mechan. Mater.* **110–116**, 177 (2011). https://doi.org/10.4028/www.scientific.net/AMM.110-116.177.

25. Z. I. Ali, O. Ebraheem, H. H. Saleh, F. H. A. Salam, and R. Sokary, *In situ* preparation of CdS/PVA nanocomposites using gamma radiation, *Polym. Eng. Sci.* **55**, 2583 (2015). https://doi.org/10.1002/pen.24151.
26. D. Das, R. Bhunia, S. Das, R. Dey, S. Hussain, A. K. Ghosh, and A. K. Pal, CdS impregnated cellulose nanocrystals/PVDF composite flexible and freestanding films: Impedance spectroscopic studies. *Polym. Eng. Sci.* **58**, 1419 (2018). https://doi.org/10.1002/pen.24735.
27. S. B. Aziz, A. Q. Hassan, S. J. Mohammed, W. O. Karim, M. F. Z. Kadir, H. A. Tajuddin, and N. N. M. Y. Chan, Structural and optical characteristics of PVA:C-Dot composites: tuning the absorption of ultra violet (UV) region. *Nanomaterials.* **9**(2), 216 (2019). https://doi.org/10.3390/nano9020216.
28. I. Apostolova, A. Apostolov, and J. Wesselinowa, Band gap tuning in transition metal and rare-earth-ion-doped TiO_2, CeO_2, and SnO_2 nanoparticles. *Nanomaterials.* **13**(1), 145 (2022). https://doi.org/10.3390/nano13010145.
29. A. S. Najm, M. S. Chowdhury, F. T. Munna, P. Chelvanathan, V. Selvanathan, M. Aminuzzaman, K. Techato, N. Amin, and Md. Akhtaruzzaman, Impact of cadmium salt concentration on CdS nanoparticles synthesized by chemical precipitation method. *Chalcogenide Lett.* **17**(11), 537 (2020). https://doi.org/10.15251/CL.2020.1711.537.
30. A. M. El-Naggar, Z. K. Heiba, M. Bakr Mohamed, A. M. Kamal, and G. Lakshminarayana, Optical investigations of $Zn_{0.75-x}$ Mn_x $Cd_{0.25}$ S/PVA/PEG blend, *J. Taibah Univ. Sci.* **16**(1), 174 (2022). https://doi.org/10.1080/16583655.2022.2037253.

الخصائص التركيبية والبصريه للتخليق الموضعي لمركبات بولي فاينيل الكحول/ كبريتيد الكادميوم النانوية باستخدام طريقة الترسيب الكيميائي والصب

حيدر جاسم فاضل[1] و حنين ثائر حسين[1]
[1]قسم الفيزياء، كلية العلوم، جامعة البصرة، البصرة، العراق

الخلاصة

تم تحضير أغشية نانوية مركبة من كحول البولي فينيل/كبريتيد الكادميوم (PVA/CdS) باستخدام طريقة الترسيب الكيميائي بالتبادل الليجاندي الموضعي، وذلك لتمييز تأثير تكوين معقدات Cd^{2+} عن تأثير تكوين جسيمات CdS النانوية على الخصائص البنيوية والبصرية لـ PVA. أُضيفت أحجام مختلفة (0.25، 0.5، 1، و2 مل) من محلول معقد رباعي أمين الكادميوم إلى PVA، ثم عولجت بكبريتيد الأمونيوم. وتم توصيف الأغشية باستخدام حيود الأشعة السينية (XRD)، ومطيافية الأشعة تحت الحمراء بتحويل فورييه (FTIR)، ومطيافية الأشعة فوق البنفسجية المرئية (UV-Vis). أكدت أنماط حيود الأشعة السينية تكوين CdS نانوي بلوري ذي بنية وورتزيت سداسية، بمتوسط حجم بلوري يبلغ حوالي 53 نانومترًا، بينما أدى تنسيق Cd2+ إلى تقليل الترتيب شبه البلوري لـ PVA. أكدت أطياف الأشعة تحت الحمراء بتقنية فورييه (FTIR) التفاعل بين أيونات الكادميوم (Cd2+) ومجموعات الهيدروكسيل في بولي فينيل الكحول (PVA)، وكشفت عن نطاقات اهتزاز مميزة لرابطة الكادميوم-الكبريت (Cd-S)، مما يؤكد تكوّن كبريتيد الكادميوم في الموقع. وأظهرت القياسات البصرية أن تكوين معقد Cd^{2+} لم يُحدث سوى تغييرات طفيفة، بينما أدى ازدياد محتوى CdS إلى تعزيز امتصاص الأشعة فوق البنفسجية بشكل ملحوظ، وخفض النفاذية إلى حوالي 0.5% عند أطوال موجية أقل من 300 نانومتر لعينة حجمها 2 مل. وانزاحت حافة الامتصاص من 5.1 إلى 3.8 إلكترون فولت، وانخفضت فجوة النطاق البصري المباشر من 5.45 إلى 4.60 إلكترون فولت. تُبين هذه النتائج أن تكوّن CdS في الموقع يوفر خصائص بصرية وعازلة قابلة للتعديل، مما يجعله مناسبًا لتطبيقات الحماية من الأشعة فوق البنفسجية، والطلاءات الضوئية والإلكترونية الضوئية.

الكلمات المفتاحيه: بولي فاينيل الكحول، مركب كبريتيد الكادميوم/بولي فينيل الكحول، الخصائص البصرية، معامل الانكسار، فجوة الطاقة.